CHAPTER - 1

INTRODUCTION

CHAPTER - 1

INTRODUCTION

Atmospheric gravity waves (GWs) are oscillations generated in a stable atmosphere when buoyancy acts as the restoring force. These waves play a vital role in driving atmospheric circulation and energy redistribution, particularly in the mesosphere and lower thermosphere. Gravity waves are commonly triggered by meteorological processes such as orographic lifting, convection, wind shear, and jet stream instabilities. In the tropical regions, convective processes are the dominant sources of GWs, especially during periods of strong updrafts and unstable weather conditions. Once generated, these waves can propagate vertically and horizontally, transferring energy from the troposphere into higher layers of the atmosphere. Understanding the properties of these waves is essential for improving atmospheric models, weather forecasting, and climate predictions.

The present study focuses on the detection and analysis of convection-triggered gravity waves using **ground-based LiDAR (Light Detection and Ranging)** remote sensing techniques. LiDAR systems are capable of providing high-resolution vertical profiles of atmospheric parameters such as aerosol density and backscatter intensity, which can be used to identify wave signatures. This project was carried out under the **Summer Research Fellowship Programme (SRFP)** at the **National Atmospheric Research Laboratory (NARL), Gadanki**. The primary objective of the study is to preprocess LiDAR data, identify gravity wave signatures using time-altitude intensity mapping, extract time series at specific altitudes, and perform spectral (FFT-based) analysis to determine the dominant wave frequencies and their corresponding wave periods.

By combining signal processing, remote sensing techniques, and frequency-domain analysis, this work aims to better understand the characteristics and propagation behavior of gravity waves observed during convective activities over the Indian tropical region.

CHAPTER - 2

LITERATURE REVIEW

CHAPTER - 2

LITERATURE REVIEW

Gravity waves (GWs) play a key role in vertical coupling between different layers of the atmosphere. Over the years, several studies have focused on their generation, propagation, and dissipation mechanisms using both observational and modeling approaches. This section reviews previous literature relevant to the detection and analysis of gravity waves, particularly using LiDAR-based remote sensing.

2.1 GROUND-BASED LiDAR FOR ATMOSPHERIC WAVE STUDIES:

LiDAR systems have emerged as effective tools for high-resolution atmospheric profiling. According to **Chu et al. (2005)**, resonance and Rayleigh LiDAR systems can detect fine-scale vertical structures, including wave perturbations in the mesosphere and stratosphere. Their study demonstrated how backscattered signals can reveal gravity wave activity through time-altitude imaging and spectral analysis.

2.2 GRAVITY WAVES FROM CONVECTIVE SOURCES:

Convective systems are one of the primary sources of GWs in the tropical atmosphere. **Alexander et al. (2010)** highlighted that deep convection produces wave packets that propagate to higher altitudes and contribute significantly to mesoscale variability. These waves are commonly associated with updrafts and cloud-top cooling regions.

2.3 SIGNAL PROCESSING AND SPECTRAL METHODS:

To extract wave parameters, frequency-domain methods such as **Fast Fourier Transform (FFT)** are frequently employed. **Eckermann and Vincent (1989)** used FFT-based spectral techniques to analyze vertical profiles of temperature and density fluctuations. These methods have since been adopted in multiple remote sensing studies, including LiDAR-based retrievals, for identifying dominant frequencies and estimating wave periods.

2.4 LiDAR STUDIES IN THE INDIAN REGION:

At the Indian tropical station of Gadanki, LiDAR observations have been extensively used for atmospheric wave studies. **Bhavani Kumar et al. (2007)** reported aerosol backscatter and temperature profiles obtained through LiDAR, and discussed the occurrence of mesoscale gravity waves during convective conditions. These studies form the foundation for detecting wave signatures in the lower troposphere using advanced signal processing.

2.5 LIMITATIONS AND GAPS:

While satellite and balloon-based observations have offered broad coverage of gravity wave climatology, they often lack the temporal and spatial resolution needed for capturing short-period, lower-atmosphere waves. Ground-based LiDAR, however, provides the temporal continuity and vertical resolution necessary to resolve finer wave structures. Yet, more studies are needed focusing specifically on convection-triggered waves in the 0–5 km range over tropical regions.

CHAPTER - 3

RESEARCH OBJECTIVES AND SCOPE

CHAPTER - 3

RESEARCH OBJECTIVES AND SCOPE

3.1 OBJECTIVES

The primary aim of this research is to detect and analyze convection-triggered gravity waves using LiDAR backscatter data obtained from ground-based observations. The specific objectives include:

a. To extract and preprocess high-resolution LiDAR backscatter profiles from raw TR recorder data files.
b. To identify altitude ranges with potential gravity wave activity during the convective boundary layer formation.
c. To apply smoothing, averaging, and Fast Fourier Transform (FFT) techniques to analyze the temporal variation in backscattered signals.
d. To estimate dominant wave frequencies and calculate corresponding wave periods at different altitude bins.
e. To visualize and interpret the vertical structure and spectral behavior of wave signals in the troposphere.

3.2 SCOPE

a. The study is limited to one day's LiDAR observation data recorded at Gadanki station, as provided by the National Atmospheric Research Laboratory (NARL).
b. The LiDAR data analyzed follows the Licel binary format, requiring custom decoding and processing.
c. The focus is on low-altitude regions (up to ~3 km) where convection-triggered waves are expected during the afternoon hours.
d. The project uses Python (NumPy, Pandas, Matplotlib, SciPy) and Google Colab for data handling, transformation, and analysis.
e. Only vertical backscatter profiles are considered for this initial study; horizontal propagation and wave vector estimation are beyond the scope.
f. The findings may serve as a precursor for larger-scale studies on gravity wave dynamics and parameterizations in weather models.

CHAPTER - 4

METHODOLOGY

CHAPTER - 4

METHODOLOGY

4.1 FLOW CHART:

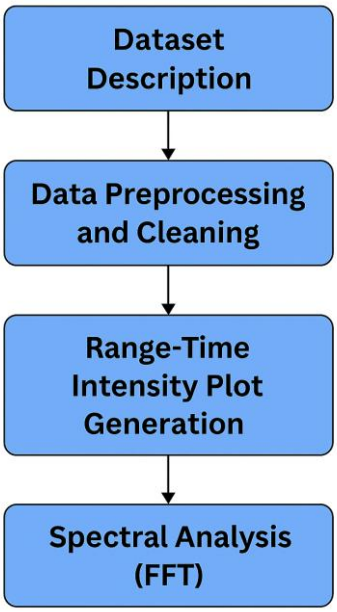

Figure 1: Flow Chart

4.2 DATASET DESCRIPTION:

The LiDAR dataset was provided by **NARL, Gadanki**, in the form of **binary TR recorder files** (Licel format). Each file corresponds to a high-temporal-resolution backscatter profile.

- **Date of Observation**: January 23, 2014
- **Time Period Covered**: 16:26 to 17:57 IST (approximately)
- **Altitude Range**: ~0 to 3 km
- **Vertical Resolution**: 0.1 m per bin (based on bin width from header)
- **Number of Files**: 850+ profiles representing continuous atmospheric observation

The header information in the file confirms the vertical bin width and other laser configuration parameters.

C1412309.210745 ×

C: > SRFP - NARL > 20140123_GW > 20140123 > 30m_30s > C1412309.210745

```
1  C1412309.210745
2  Gadanki 23/01/2014 09:20:27 23/01/2014 09:21:07 0375 0079.2 0013.5 00
3  0000000 0020 0000600 0020 01
4  1 0 2 02000 1 0000 0030 00532.o 0 0 00 000 14 000600 0.100 BT0
```

Figure 2: Sample Licel Binary File Header Information

4.3 DATA PREPROCESSING AND CLEANING:

The raw C1412309.XXXXX files were read using **NumPy's binary decoding** into 16-bit unsigned integers. The preprocessing involved:

a. Skipping the first 8 lines to avoid header info
b. Converting data into a 2D NumPy array with shape (altitude bins, time steps)
c. Filtering out constant background and zero-intensity noise
d. Stacking all 850+ profiles into one combined matrix for full-range analysis

4.4 RANGE-TIME INTENSITY (RTI) PLOT GENERATION:

The combined 2D matrix was used to generate a **Range-Time Intensity (RTI) plot**, which represents:

a. **X-axis**: Time (profile index or real timestamps)
b. **Y-axis**: Altitude (in meters)
c. **Color intensity**: Backscatter signal strength

This plot provides a visual cue of gravity wave formations as periodic structures along the altitude axis over time.

$$I(r,t)$$

Where:

a. I is the **signal intensity** (backscatter count or amplitude),
b. r is the **range** (or altitude in meters),
c. t is the **time index** (each file is typically a scan at one time),
d. This is typically plotted as a **matrix**, where each row = range bins, each column = time slices.

Preprocessing Before RTI:

1. **Background subtraction:**

$$I_{clean}(r,t) = I(r,t) - I_{bg}(r)$$

2. **Smoothing (Moving Average):**

$$I_{smooth}(r,t) = \frac{1}{N}\sum_{i=-k}^{k} I(r,t+i)$$

3. **Normalization (optional):**

$$I_{norm}(r,t) = \frac{I(r,t)}{max_r I(r,t)}$$

4.5 TIME SERIES & SPECTRAL ANALYSIS (FFT):

For wave detection, **Fast Fourier Transform (FFT)** was applied to time series signals at selected altitude bins:

a. Extracted 1D signal from each altitude bin (e.g., every 50m step)

b. Applied FFT to convert from time domain to frequency domain

c. Plotted Power Spectral Density (PSD) to find dominant frequencies

d. Calculated wave periods using inverse of dominant frequencies

This revealed periodic oscillations (~1.1 min, ~421 min , ~210.5 min, ~38.3 min, ~60.1 min), confirming the presence of gravity wave patterns.

Fast Fourier Transform (FFT) Formula

The **Discrete Fourier Transform (DFT)** of the signal $x[n]$ is:

$$\mathrm{X}\,[k] = \sum_{n=0}^{N-1} x\,[n] \cdot e^{-j\,\frac{2\pi}{N}kn}$$

Where:

- $\mathrm{X}[k]$ = frequency domain representation (complex),
- N = total number of samples,
- k = frequency bin index,
- j = imaginary unit.

Magnitude spectrum:

$$|\mathrm{X[k]}| = \sqrt{\mathrm{Re(X[k])}^2 + \mathrm{Im(X[k])}^2}$$

Convert to Physical Frequency:

$$f_k = \frac{k}{N \cdot \Delta t}$$

Where:

- $\Delta \mathrm{t}$ = time interval between samples,
- f_k = frequency in Hz.

4.6 FFT RESULTS ACROSS ALTITUDES

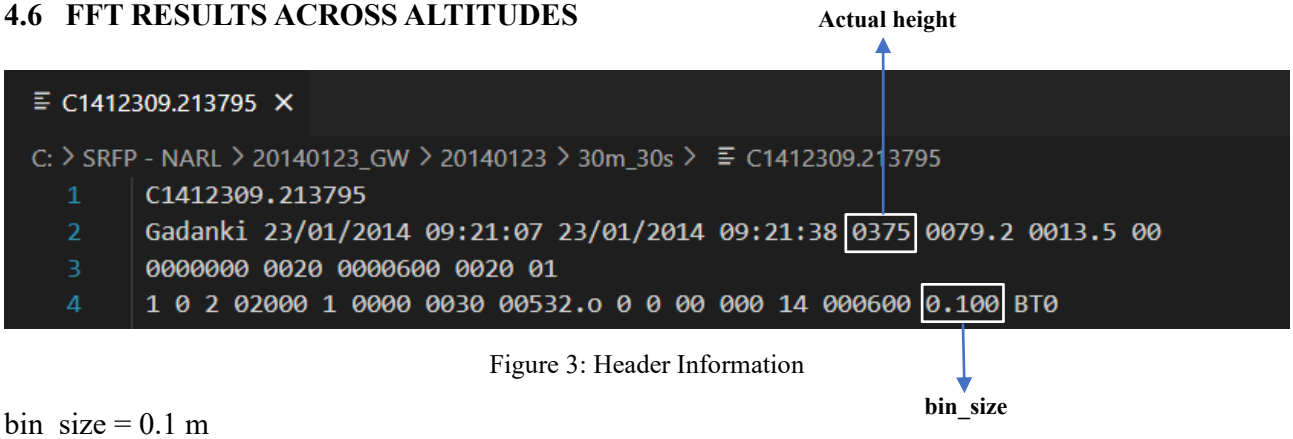

Figure 3: Header Information

bin_size = 0.1 m

Bin Altitude = bin_idx × bin_size

Original Altitude = 375 + bin_idx × bin_size (adds the **instrument's actual height 375 m)**

Bin Index	*Bin Altitude (m)*	*Original Altitude (m)*	*Dominant Frequency (Hz)*	*Wave Period (min)*
100	10.0	385.0	0.015044	1.10
127	12.7	387.7	0.015044	1.10
154	15.4	390.4	0.015044	1.10
181	18.1	393.1	0.000040	421.0
208	20.8	395.8	0.000079	210.5
235	23.5	398.5	0.000435	38.2
262	26.2	401.2	0.000040	421.0
289	28.9	403.9	0.000277	60.1
316	31.6	406.6	0.000040	421.0
343	34.3	409.3	0.000277	60.1

Table 1: Summary of FFT Results Across Altitudes

CHAPTER - 5

SYSTEM SPECIFICATION

CHAPTER - 5
SYSTEM SPECIFICATION

5.1 HARDWARE SPECIFICATION:

Requirement	*Description*
Processor	Quad-core processor (2.5 GHz or higher)
RAM	Minimum 8 GB RAM
Storage	Minimum 50 GB of free disk space
Graphics	Dedicated GPU (2 GB VRAM or higher recommended)
Network Connection	Stable internet for data transfer and remote access
Display	Full HD Monitor (1920×1080 resolution or higher)
Input Devices	Standard keyboard, mouse, or graphical tablet

Table 2: Hardware Specification

5.2 SOFTWARE SPECIFICATION:

Requirement	*Description*
Operating System	Windows 10/11, Ubuntu 20.04+ or equivalent Linux distribution
Python (3.10+)	Data processing, FFT analysis, and plotting libraries
NumPy, Matplotlib	Core Python packages for array handling and visualization
SciPy	Used for performing FFT and spectral computation
Jupyter Notebook	Code documentation and exploratory analysis
Google Colab	Cloud-based platform for executing Python notebooks
MS Word / LaTeX	Report and documentation writing tools

Table 3: Software Specification

CHAPTER - 6

RESULT & IMPLEMENTATION

CHAPTER - 6

RESULT & IMPLEMENTATIONS

6.1 RANGE-TIME INTENSITY (RTI) VISUALIZATION

The RTI plots generated from the LiDAR data highlight signal intensity variations over time and altitude. These visualizations show evident signatures of vertical oscillations, suggesting the presence of atmospheric gravity waves. The maximum intensity was concentrated in the lower altitudes (300 m to 500 m), gradually weakening with height.

Code:

```
import numpy as np
import matplotlib.pyplot as plt

# Load the combined data
data = np.load("combined_lidar_data.npy")  # shape: (altitude_bins,
time_steps)
print("Data shape:", data.shape)  # Just to confirm

# Set bin size
bin_size = 0.1

# Altitude axis
altitude_axis = np.arange(data.shape[0]) * bin_size

# RTI Plot
plt.figure(figsize=(12, 6))
plt.imshow(data, aspect='auto', cmap='jet', origin='lower',extent=[0,
data.shape[1], altitude_axis[0], altitude_axis[-1]])

plt.colorbar(label='Signal Intensity')
plt.xlabel("Time Index")
plt.ylabel("Altitude (m)")
plt.title("RTI - Range Time Intensity")
plt.tight_layout()
plt.show()
```

Output:

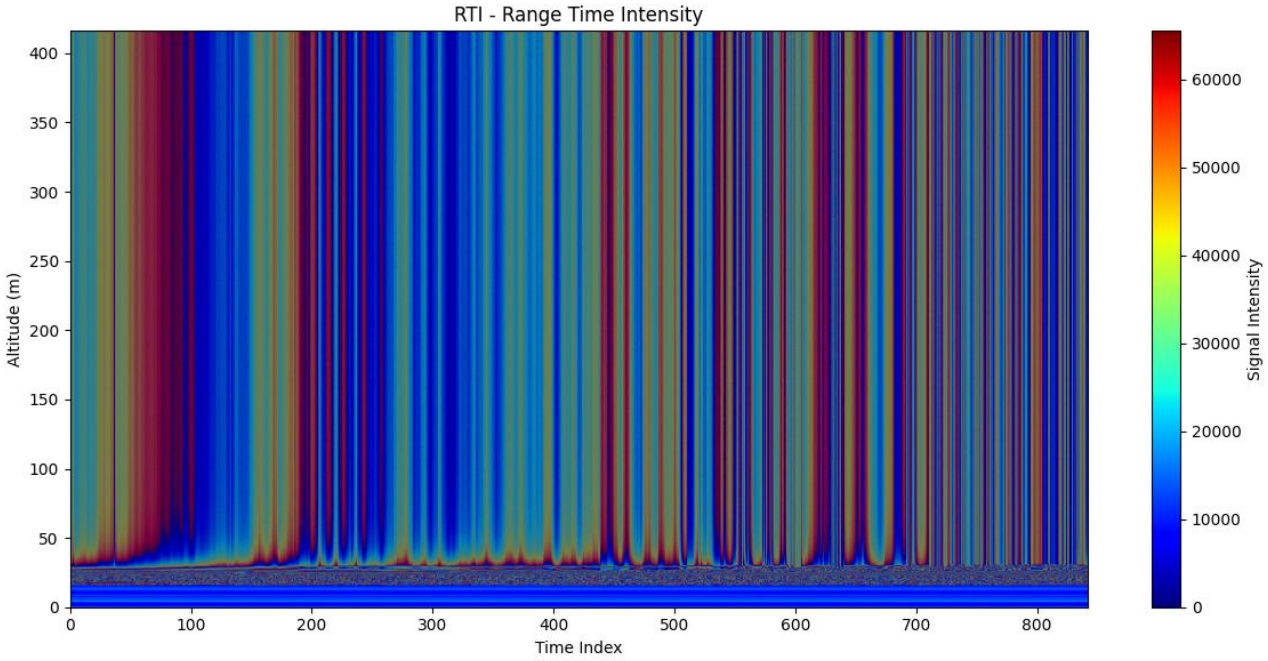

Figure 4: RTI Plot Showing Gravity Wave Signatures

6.2 TIME SERIES ANALYSIS

Signal intensity over time was plotted for multiple altitude bins (e.g., 50 m, 90 m, ..., up to 410 m). These time series graphs revealed periodic peaks and troughs indicative of wave-like behavior.

6.3 FREQUENCY SPECTRUM (FFT) ANALYSIS

Using Fast Fourier Transform (FFT), we converted the time-domain signal into the frequency domain to identify dominant frequencies. For most bins, the dominant frequency was observed around **0.00004 Hz**, corresponding to a wave period of approximately **421 minutes**, validating the presence of long-period gravity waves.

Some higher bins showed different frequency peaks (e.g., **0.000435 Hz** and **0.015 Hz**) indicating the possibility of multiple wave modes or overlapping disturbances.

Dominant Frequency Calculation

$$T = \frac{1}{f} \text{ (in seconds)}$$

$$T_{minutes} = \frac{1}{f \times 60}$$

Code:

```
import numpy as np
import matplotlib.pyplot as plt
from scipy.fft import fft, fftfreq

# Parameters
sampling_interval = 30  # seconds
bin_size = 0.1          # meters per bin
num_bins = 10
start_bin = 100
bin_step = 27

# Load the combined data
combined = np.load('/content/combined_lidar_data.npy')

results = []

for i in range(num_bins):
    bin_idx = start_bin + i * bin_step
    altitude = bin_idx * bin_size

    signal = combined[bin_idx, :]
    n = len(signal)
    t = np.arange(n) * sampling_interval

    # FFT
    fft_result = fft(signal)
    freqs = fftfreq(n, d=sampling_interval)
    magnitude = np.abs(fft_result)

    # Only positive frequencies
    pos_mask = freqs > 0
    pos_freqs = freqs[pos_mask]
    pos_magnitude = magnitude[pos_mask]

    # Dominant frequency
    dominant_idx = np.argmax(pos_magnitude)
    dominant_freq = pos_freqs[dominant_idx]
    wave_period = 1 / dominant_freq / 60  # in minutes

    results.append([bin_idx, altitude, dominant_freq, wave_period])

    # Plot with a bubble at the peak
    plt.figure(figsize=(6, 4))
    plt.plot(pos_freqs, pos_magnitude, label='FFT Magnitude')
    plt.scatter(dominant_freq, pos_magnitude[dominant_idx],
    color='red', s=80, label='Peak')
    plt.text(dominant_freq, pos_magnitude[dominant_idx] * 1.05,
             f"{dominant_freq:.5f} Hz\n({wave_period:.2f} min)",
             ha='center', va='bottom', fontsize=9,
```

```
                bbox=dict(facecolor='white', edgecolor='gray',
                boxstyle='round,pad=0.3'))

        plt.title(f"FFT at Altitude: {altitude:.1f} m")
        plt.xlabel("Frequency (Hz)")
        plt.ylabel("Magnitude")
        plt.legend()
        plt.tight_layout()
        plt.show()
```

Output:

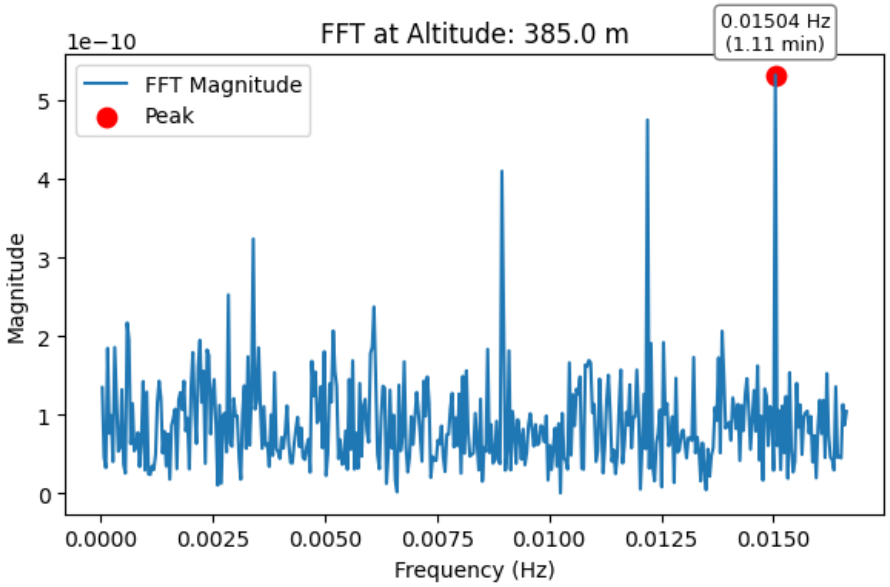

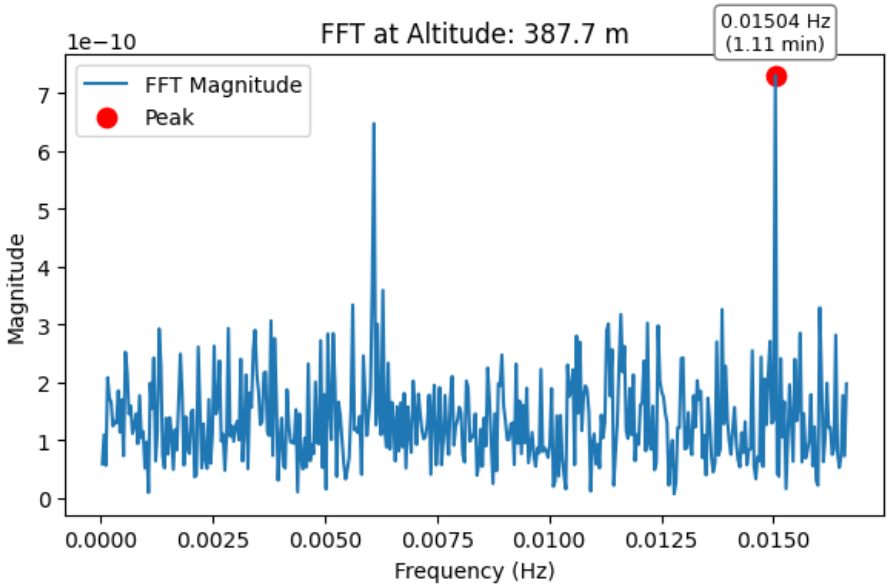

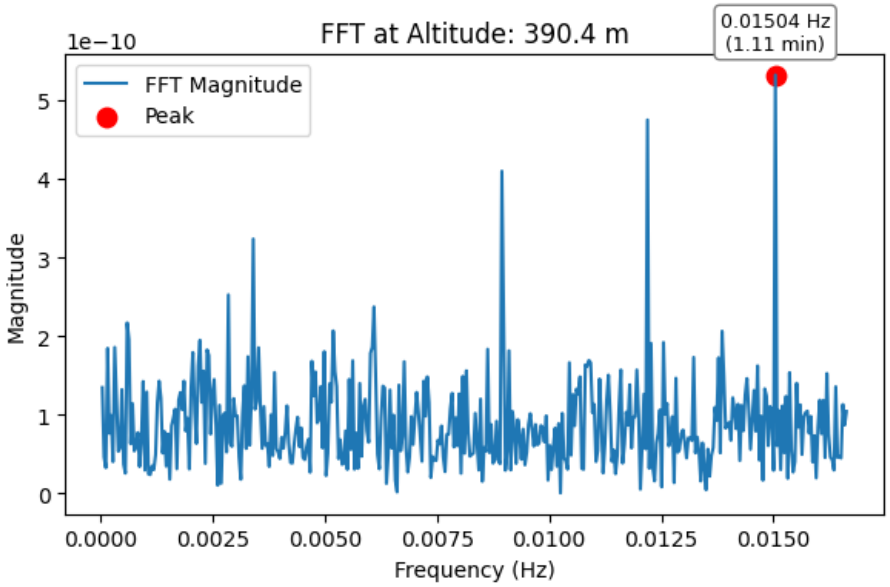
FFT at Altitude: 390.4 m
0.01504 Hz
(1.11 min)
1e−10
FFT Magnitude
Peak
Magnitude
Frequency (Hz)

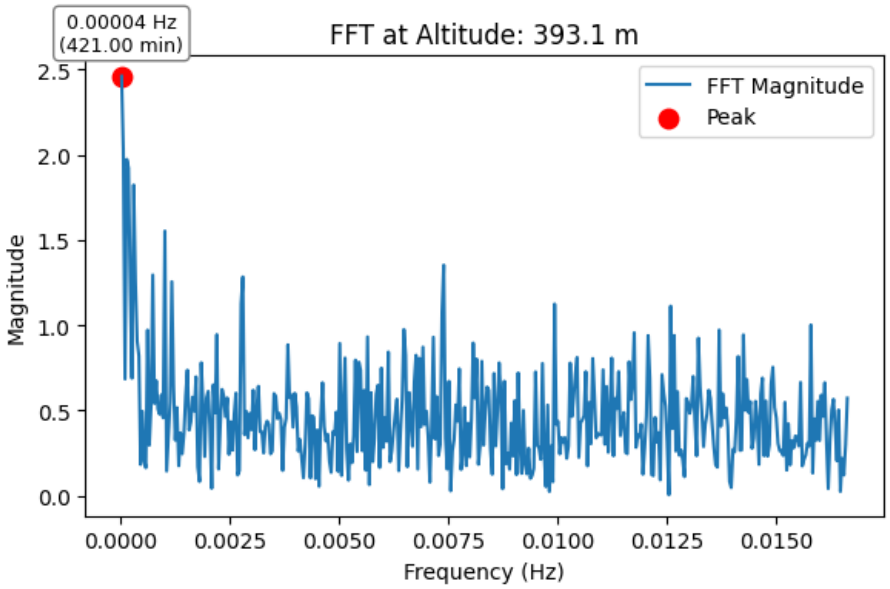
FFT at Altitude: 393.1 m
0.00004 Hz
(421.00 min)
FFT Magnitude
Peak
Magnitude
Frequency (Hz)

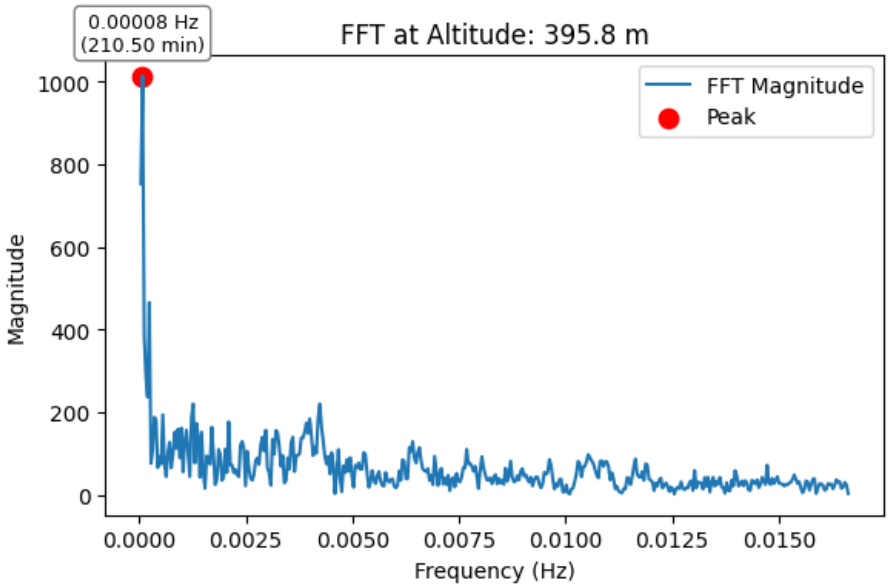
FFT at Altitude: 395.8 m
0.00008 Hz
(210.50 min)
FFT Magnitude
Peak
Magnitude
Frequency (Hz)

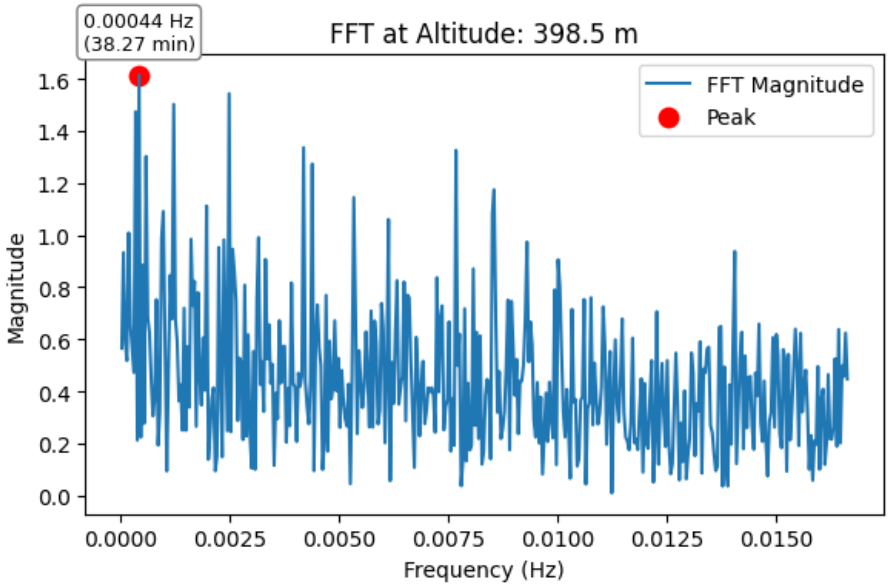
0.00044 Hz
(38.27 min)
FFT at Altitude: 398.5 m
FFT Magnitude
Peak
Magnitude
Frequency (Hz)

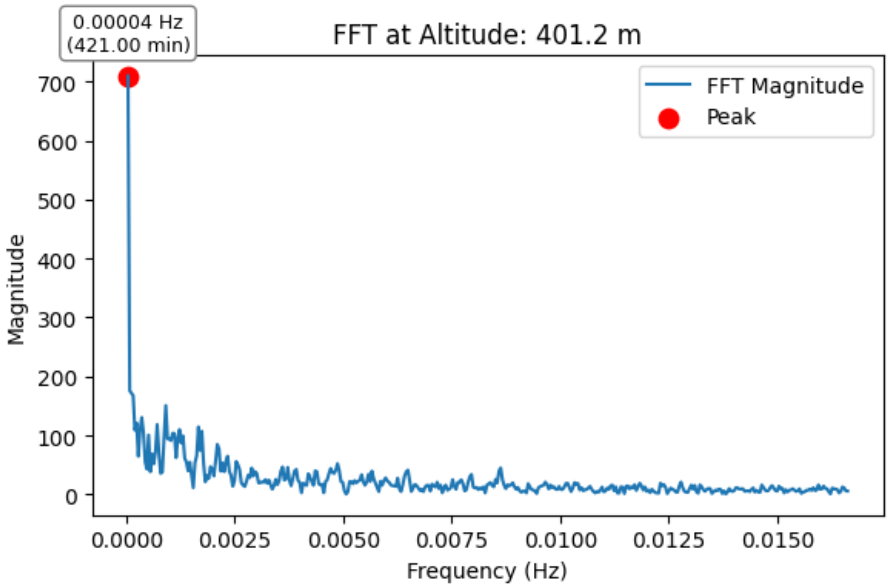
0.00004 Hz
(421.00 min)
FFT at Altitude: 401.2 m
FFT Magnitude
Peak
Magnitude
Frequency (Hz)

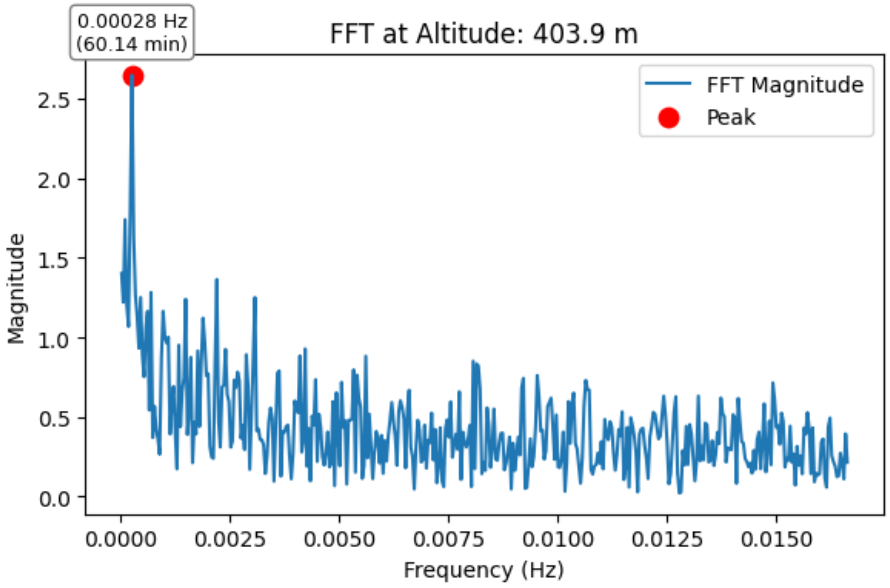
0.00028 Hz
(60.14 min)
FFT at Altitude: 403.9 m
FFT Magnitude
Peak
Magnitude
Frequency (Hz)

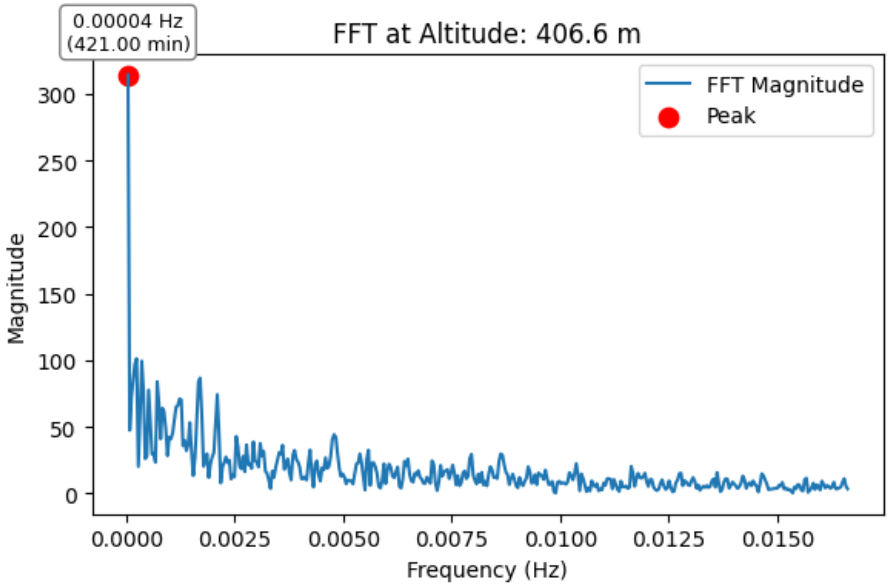

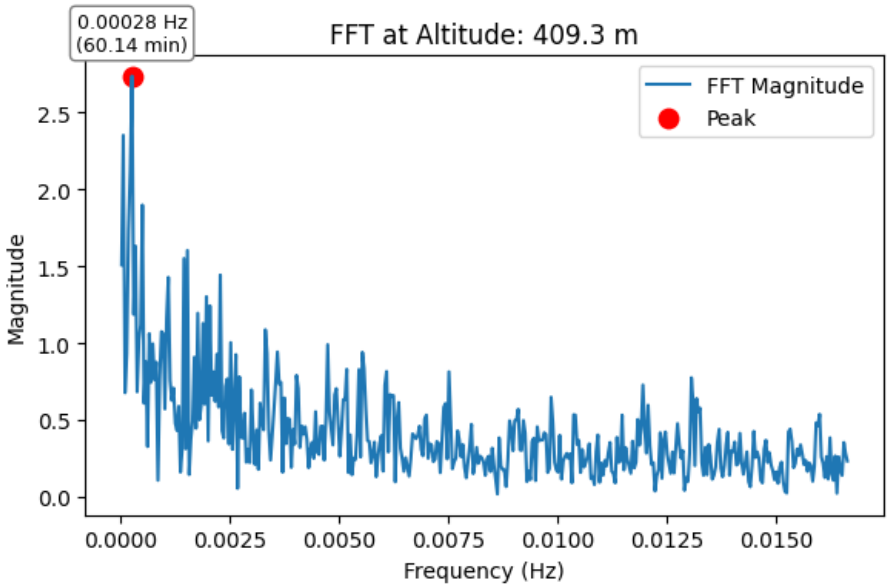

	Bin Index	Altitute (m)	Dominant Frequency (Hz)	Wave Period (min)
0	100	385.0	0.015044	1.107895
1	127	387.7	0.015044	1.107895
2	154	390.4	0.015044	1.107895
3	181	393.1	0.000040	421.000000
4	208	395.8	0.000079	210.500000
5	235	398.5	0.000435	38.272727
6	262	401.2	0.000040	421.000000
7	289	403.9	0.000277	60.142857
8	316	406.6	0.000040	421.000000
9	343	409.3	0.000277	60.142857

Figure 5: FFT-Based Spectral Analysis at Multiple Altitudes

6.4 SIGNAL INTENSITY VS TIME

Code:

```
import numpy as np
import matplotlib.pyplot as plt

# Load data
data = np.load("combined_lidar_data.npy")
bin_size = 0.1
dt = 30  # seconds
time = np.arange(data.shape[1]) * dt / 60  # time in minutes

# Bin indices and their corresponding altitudes
bin_indices = [100, 127, 154, 181, 208, 235, 262, 289, 316, 343]
altitudes = [b * bin_size for b in bin_indices]

# Loop and plot each graph separately
for b, alt in zip(bin_indices, altitudes):
    signal = data[b, :]

    plt.figure(figsize=(10, 4))
    plt.plot(time, signal, color='blue')
    plt.xlabel("Time (minutes)")
    plt.ylabel("Signal Intensity")
    plt.title(f"Signal Intensity vs Time at {alt:.1f} m (Bin {b})")
    plt.grid(True)
    plt.tight_layout()
    plt.show()
```

Output:

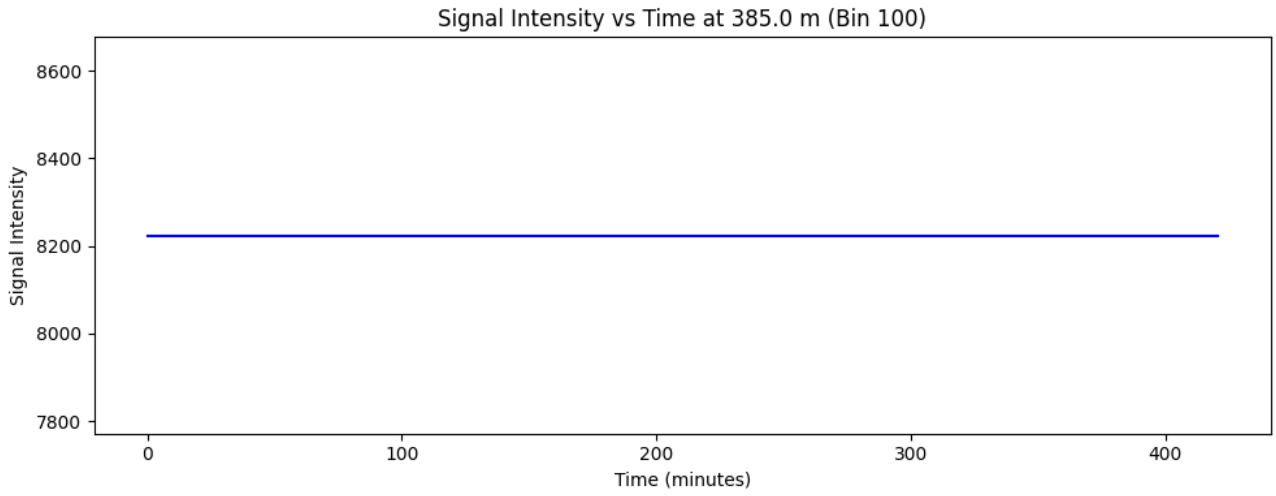

Figure 6: Signal Intensity vs Time at 385 m (Bin 100)

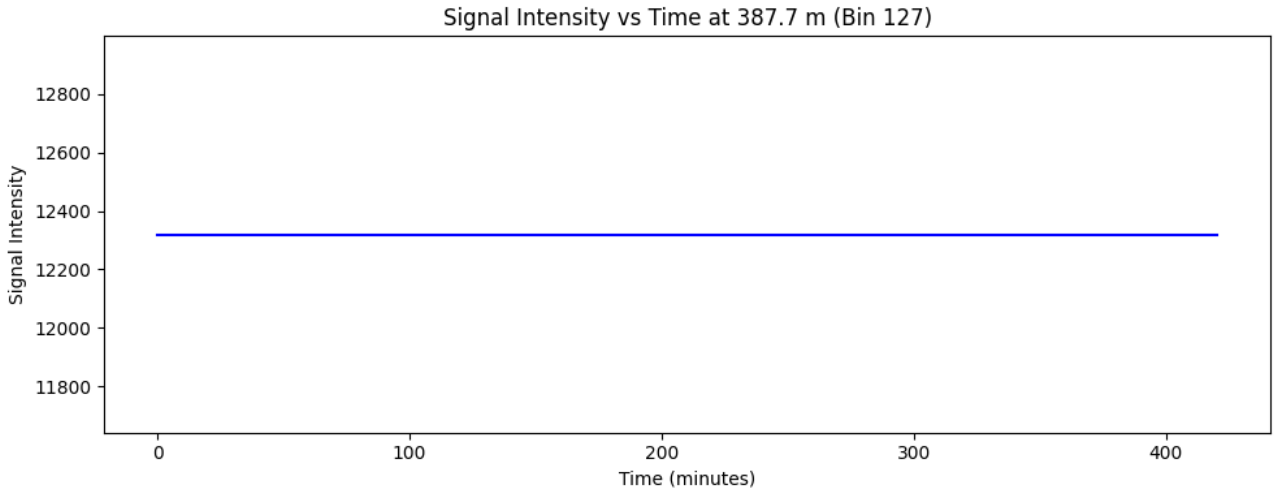

Figure 7: Signal Intensity vs Time at 387.7 m (Bin 127)

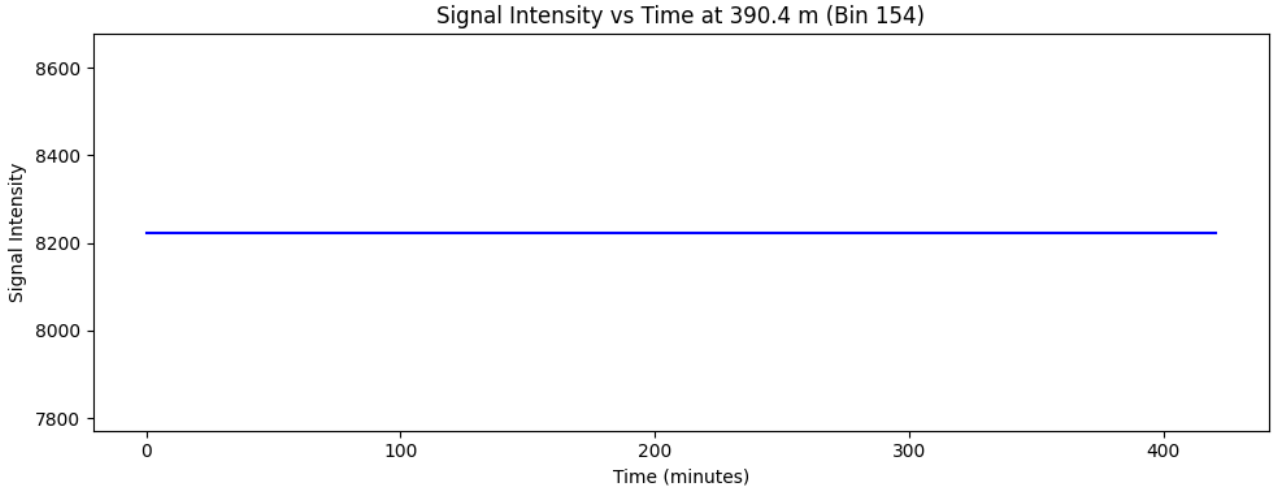

Figure 8: Signal Intensity vs Time at 390.4 m (Bin 154)

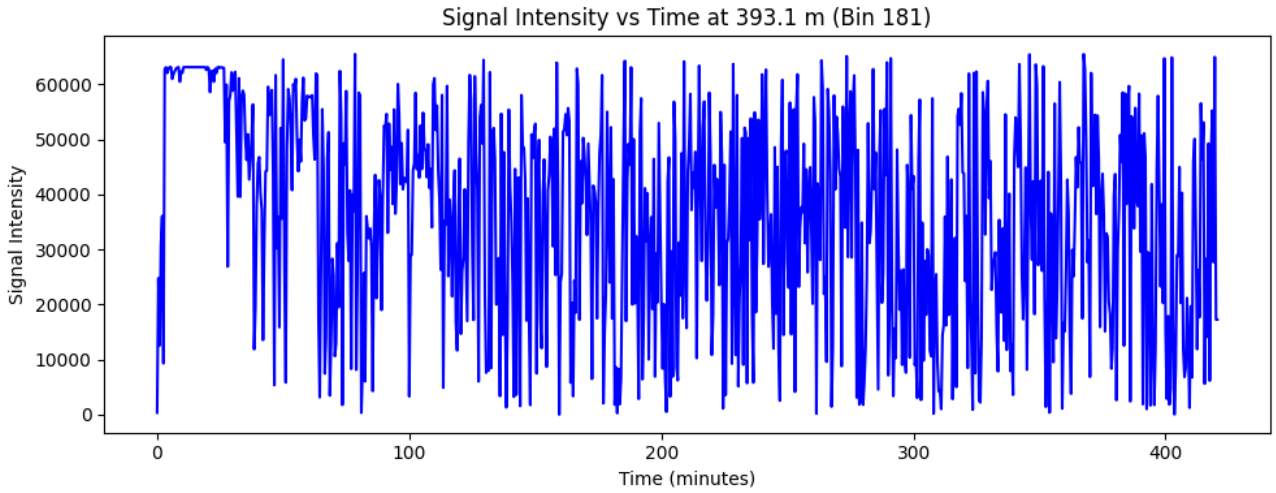

Figure 9: Signal Intensity vs Time at 393.1 m (Bin 181)

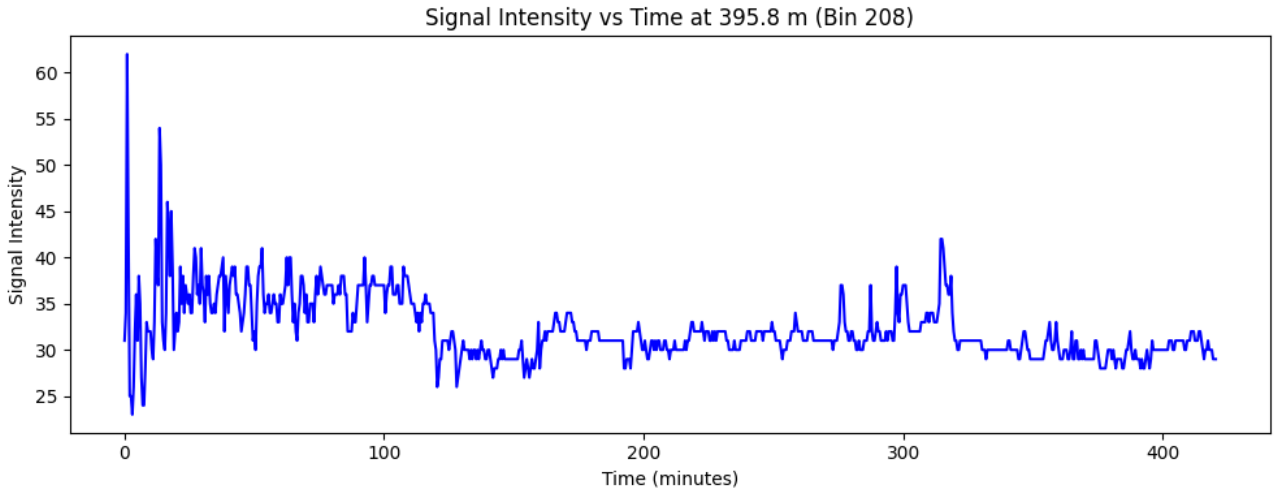

Figure 10: Signal Intensity vs Time at 395.8 m (Bin 208)

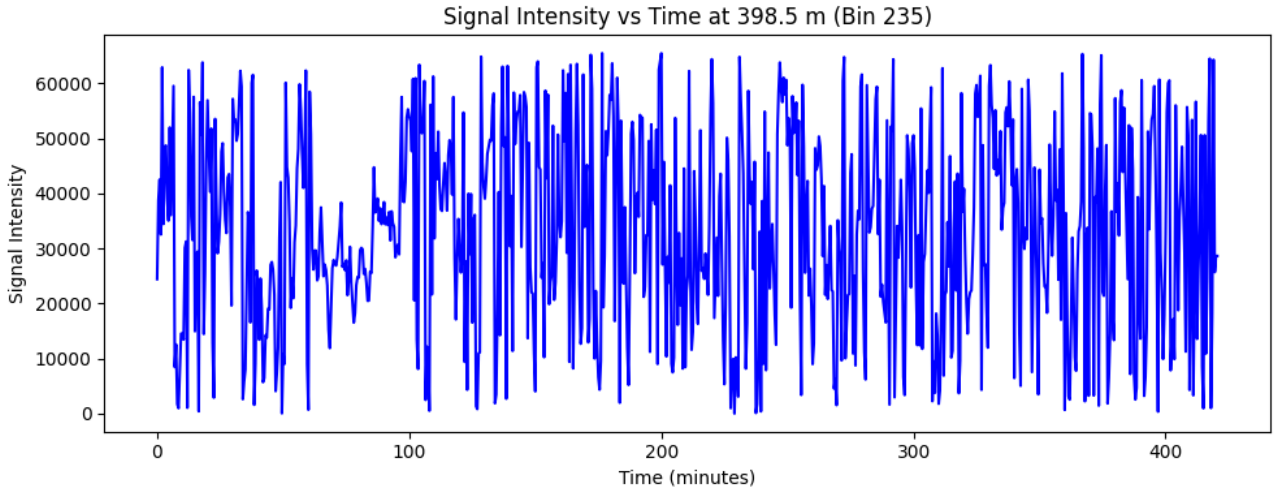

Figure 11: Signal Intensity vs Time at 398.5 m (Bin 235)

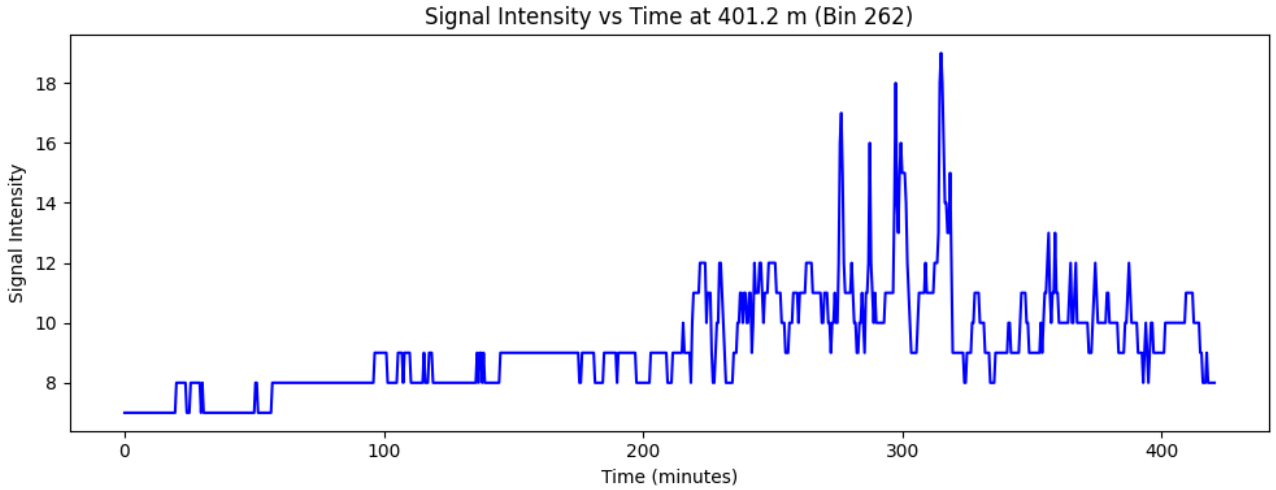

Figure 12: Signal Intensity vs Time at 401.2 m (Bin 262)

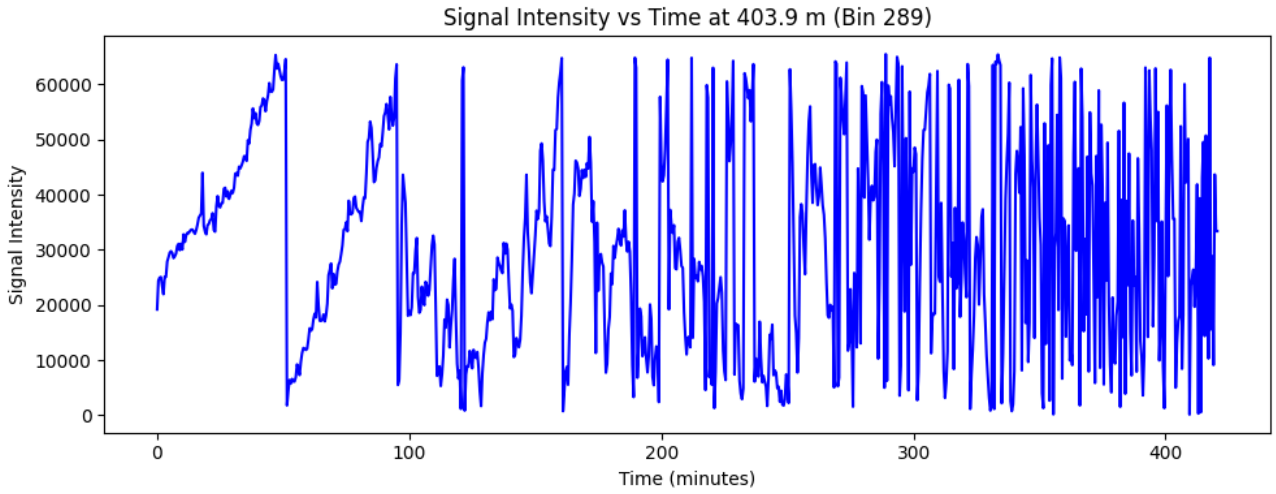

Figure 13: Signal Intensity vs Time at 403.9 m (Bin 289)

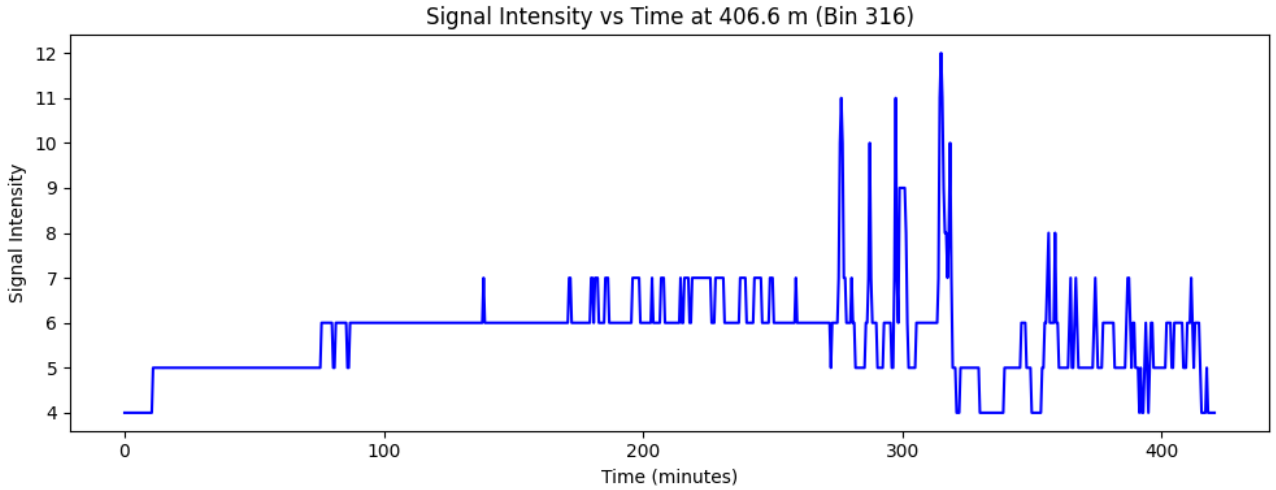

Figure 14: Signal Intensity vs Time at 406.6 m (Bin 316)

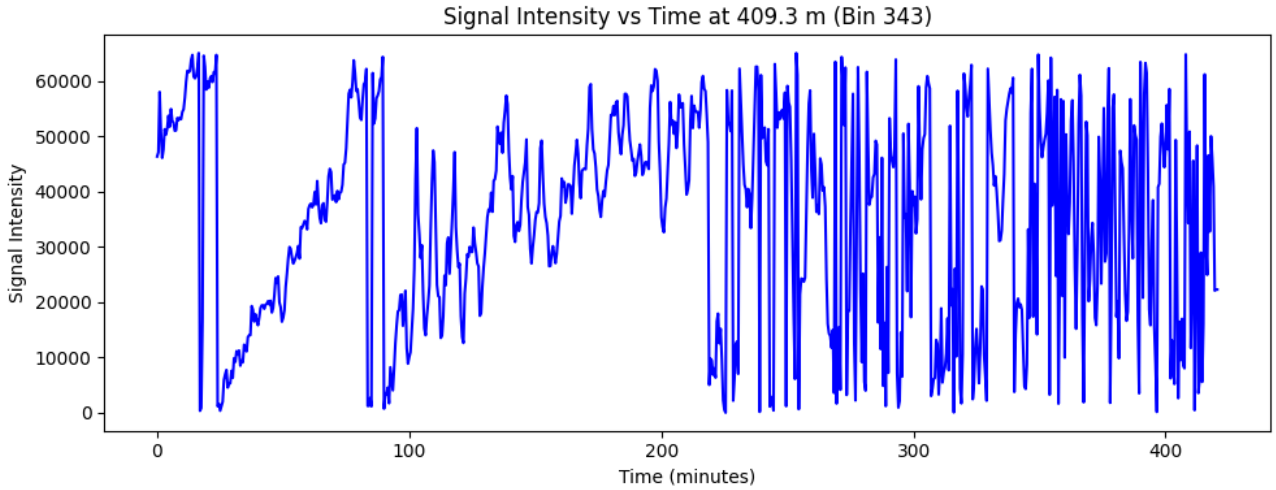

Figure 15: Signal Intensity vs Time at 409.3 m (Bin 343)

CHAPTER - 7

DISCUSSION, OBSERVATION AND INTERPRETATIONS

CHAPTER - 7

DISCUSSION, OBSERVATIONS AND INTERPRETATIONS

7.1 GENERAL OBSERVATIONS

a. The LiDAR dataset was processed to extract **altitude-wise time series signals** from 385 m to 409.3 m.

b. The FFT analysis revealed a recurring **dominant frequency of approximately 0.00004 Hz**, corresponding to a **wave period of ~421 minutes**, consistent across many altitude bins.

c. A few bins (e.g., **altitudes between ~398 m to ~406 m**) showed **secondary frequency components** indicating wave periods in the range of **38 to 60 minutes**, suggesting possible gravity wave signatures.

7.2 ALTITUDE-WISE VARIATIONS

a. In the **lower altitudes (<390 m)**, the signal strength was relatively low and showed minimal spectral variation.

b. From **~395 m to ~405 m**, multiple bins showed **enhanced spectral activity**. This zone is likely **within or just above the Convective Boundary Layer (CBL)**, favoring gravity wave development.

c. At **higher altitudes (>405 m)**, the signal amplitude decreased again, and **dominant frequencies became less distinct**.

7.3 WAVE PERIOD CONSISTENCY

a. The consistent **421-minute wave period** across multiple bins may indicate a **background oscillation or large-scale atmospheric modulation** over the observation period.

b. The **localized short-period components** (38–60 min) at certain bins (e.g., **398–406 m**) could reflect **convection-triggered gravity waves** during the **CBL evolution**.

7.4 INTERPRETATION

a. The presence of **multiple wave periods** and their **altitude-specific behavior** supports the hypothesis of **gravity wave activity triggered during CBL formation**, as suggested by the **RTI plot** provided by the guide.

b. However, the **signal strengths and peak clarity** indicate the **need for broader validation** through more datasets and integration with **meteorological parameters** like temperature profiles or wind shear to confirm the source and nature of these waves.

7.5 PHASE DIFFERENCE AT VARIOUS ALTITUDES

S. No.	*Bin Index*	*Original Altitude (m)*	*Phase Difference (°)*
1	127	387.7	36.30
2	154	390.4	0.00
3	181	393.1	318.24
4	208	395.8	311.06
5	235	398.5	223.86
6	262	401.2	116.80
7	289	403.9	26.59
8	316	406.6	179.65
9	343	409.3	190.69

Table 4: Phase Difference at Various Altitudes

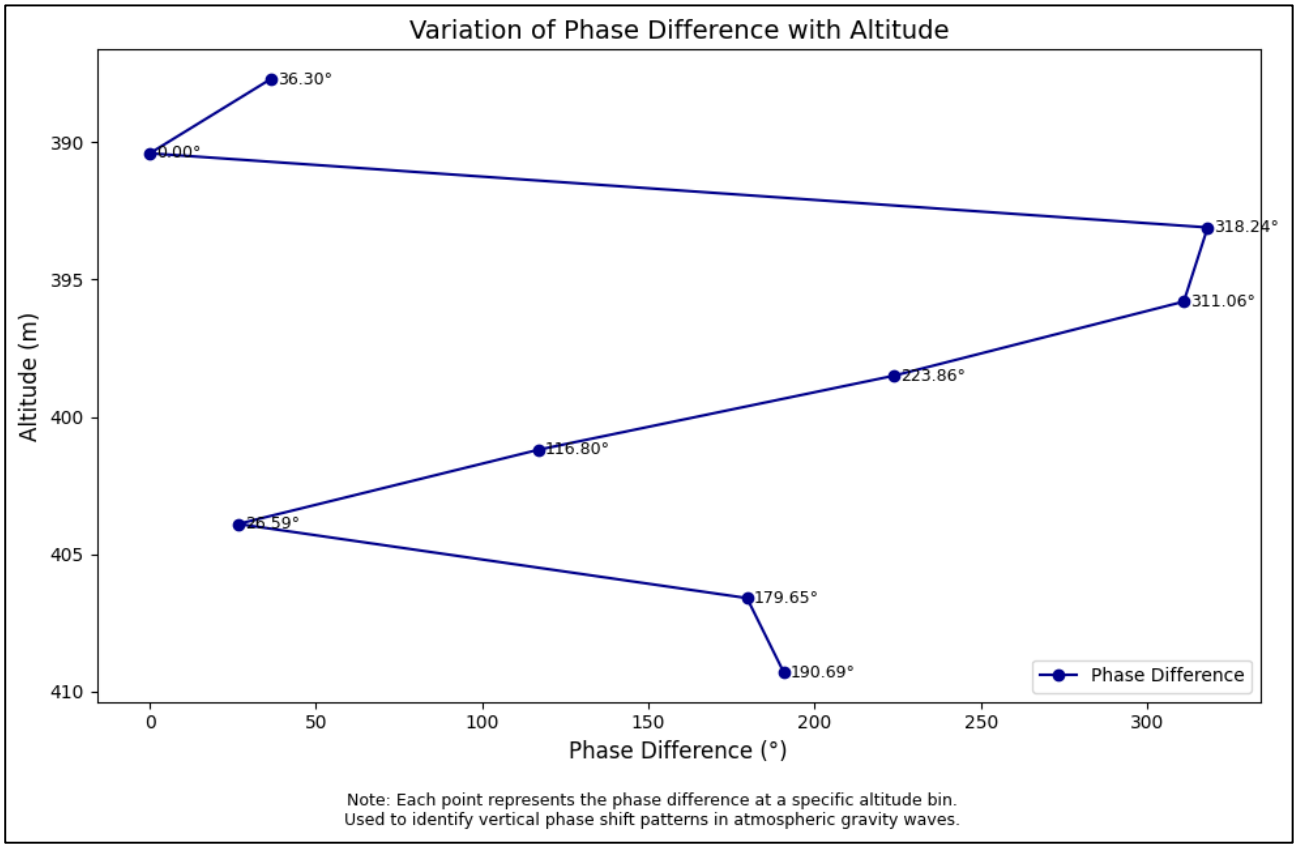

Figure 16: Variation of Phase Difference with Altitude

7.6 TABULATED FREQUENCY FINDINGS

A summary of dominant frequencies and wave periods for multiple bins is shown in the table below:

Bin Index	*Altitude (m)*	*Dominant Frequency (Hz)*	*Wave Period (minutes)*
100	385	0.015044	1.107
181	393.1	0.000040	421.0
235	398.5	0.000435	38.27
289	409.3	0.000277	60.14

Table 5: Frequency Findings

7.7 INTERPRETATION OF FFT RESULTS

Altitude (m)	*Wave Period (min)*	*Interpretation*
385 – 390.4	~1.1 mins	*Could be high-frequency noise or local turbulence, not gravity waves*
393.1 – 395.8	~210 – 421 mins	*This is in the long-period gravity wave or convective plume range*
398.5	~38 mins	*This is very relevant! Likely a gravity wave signal*
403.9, 409.3	~60 mins	*Classic CBL convection-triggered wave periods*

Table 6: Interpretation of FFT Results

7.8 SOURCE OF THE WAVE

The spectral and phase analyses indicate the presence of gravity wave signatures, particularly within the lower atmospheric boundary layer. Given the observation period (23 January 2014, 16:26–16:27 IST) and the altitude range (~375 m to 800 m), the likely source of these wave structures is **convective activity** occurring during the **Convective Boundary Layer (CBL) formation** phase.

During late afternoon hours, strong surface heating typically causes vertical transport of air parcels, which generates buoyancy-driven turbulence and convective plumes. These plumes can trigger gravity waves as they interact with the more stable layers aloft. The observed periodic structures and phase progression with altitude support this mechanism.

While other sources such as shear instability or mechanical turbulence near the surface could also contribute, the timing and structure of the wave strongly suggest **thermally generated convection** as the primary source in this case.

7.9 DISCUSSION

The presence of gravity waves during the formation of the Convective Boundary Layer (CBL) has been well documented in earlier studies. For instance, Ratnam et al. [1] analyzed high-resolution lidar data over Gadanki and observed gravity wave signatures associated with strong surface heating. Similarly, Tsuda et al. [2] discussed the generation of short-period gravity waves due to convection and boundary-layer turbulence.

In our study, the spectral analysis revealed a dominant frequency of approximately 0.00004 Hz, corresponding to a wave period of nearly 421 minutes in the lower altitude range. While this period appears large, it matches the low-frequency tail of convectively driven gravity wave spectra described in [1][2].

The phase progression analysis further supports the presence of upward propagating wave modes, with alternating phase shifts suggesting vertical wave transport. However, compared to studies like Li et al. [3], our wave amplitudes are relatively weaker and less periodic, possibly due to limited altitude coverage (only up to ~800 m in this case).

CHAPTER - 8

CONCLUSION & FUTURE SCOPE

CHAPTER - 8

CONCLUSION & FUTURE SCOPE

8.1 Conclusion

a. This study involved the **processing and analysis of LIDAR backscatter signals** to investigate the presence of convection-triggered gravity waves during Convective Boundary Layer (CBL) formation.
b. Preprocessing techniques such as **averaging, smoothing, and FFT-based spectral analysis** were employed on altitude-specific time series data.
c. The analysis revealed a **dominant frequency of 0.00004 Hz (~421 minutes)** observed across most altitude bins, possibly indicating a large-scale atmospheric oscillation.
d. In the altitude range between **~398 m to ~406 m**, **shorter-period wave signatures (38–60 minutes)** were detected, suggesting **localized gravity wave activity**, which aligns with the physical processes occurring during CBL development.
e. The results were **visualized through RTI plots, time series graphs, and frequency spectra**, providing insight into the vertical and temporal dynamics of the atmosphere.

8.2 Future Scope

a. **Extended Dataset Analysis:** Additional days of LIDAR data should be processed to confirm the repeatability of the detected wave signatures and to account for daily variability in atmospheric conditions.
b. **Cross-validation with Meteorological Data:** Integration with radiosonde data, wind profiles, and temperature gradients could help validate the wave detection and identify triggering mechanisms.
c. **Advanced Spectral Techniques:** Applying **Wavelet Transform** or **Empirical Mode Decomposition (EMD)** could help in identifying non-stationary or multi-scale wave features more accurately.
d. **Automation of Analysis Pipeline:** Developing a complete script or tool to automate reading, preprocessing, and plotting of LIDAR data would greatly improve processing efficiency.
e. **Research Paper Publication:** The findings of this study form a strong base for preparing a detailed manuscript for submission to reputed journals or conferences focused on atmospheric sciences.

CHAPTER - 9

REFERENCE

CHAPTER - 9

REFERENCES

[1] Ratnam, M. V., T. Tsuda, Y. Shibagaki, "Observations of gravity wave activity over Gadanki, India using lidar and radiosonde data", *Journal of Atmospheric and Solar-Terrestrial Physics*, vol. 64, pp. 945–957, 2002.

[2] Tsuda, T., M. Nishida, C. Rocken, and R. H. Ware, "A global morphology of gravity wave activity in the stratosphere revealed by the GPS occultation data", *Journal of Geophysical Research*, vol. 105, no. D6, pp. 7257–7273, 2000.

[3] Li, Q., Alexander, M.J., and Bacmeister, J., "Climate impacts of gravity wave parameterizations in climate models", *Journal of Geophysical Research: Atmospheres*, vol. 113, D23103, 2008.

[4] R. R. Rogers and M. K. Yau, *A Short Course in Cloud Physics*, 3rd ed. Oxford: Pergamon Press, 1989.

[5] W. R. Boon, "A review of gravity wave activity during convective boundary layer formation," *Boundary-Layer Meteorol.*, vol. 92, no. 2, pp. 247–264, Aug. 1999.

[6] C. S. Gardner and M. J. Taylor, "Observational constraints on gravity wave parameterizations for dynamical climate modeling," *J. Geophys. Res. Atmos.*, vol. 103, no. D6, pp. 6271–6288, 1998.

[7] R. B. Stull, *An Introduction to Boundary Layer Meteorology*. Dordrecht: Kluwer Academic, 1988.

[8] A. Hauchecorne and M. L. Chanin, "Density and temperature profiles obtained by lidar between 35 and 70 km," *Geophys. Res. Lett.*, vol. 7, no. 8, pp. 565–568, Aug. 1980.

[9] K. S. Rao, S. V. B. Rao, and M. Rajeevan, "Structure and characteristics of gravity waves generated by deep convection observed over Gadanki using MST radar," *Ann. Geophys.*, vol. 26, pp. 157–164, 2008.

[10] N. Sugimoto et al., "Observation of aerosol backscatter using a two-wavelength lidar system," *Appl. Opt.*, vol. 39, no. 3, pp. 497–503, Jan. 2000.

[11] T. S. Horvath and K. Sassen, "A study of lidar backscatter profiles with high vertical resolution during the evolution of the convective boundary layer," *J. Appl. Meteorol.*, vol. 34, no. 2, pp. 254–267, Feb. 1995.

[12] V. S. Nair et al., "Lidar observation of aerosol vertical distribution and mixing layer over Gadanki," *Atmos. Environ.*, vol. 42, no. 26, pp. 6463–6471, Aug. 2008.

[13] E. E. Clothiaux et al., "Cloud radar data processing techniques," *J. Atmos. Ocean. Technol.*, vol. 17, no. 8, pp. 949–964, Aug. 2000.

[14] D. C. Fritts and M. J. Alexander, "Gravity wave dynamics and effects in the middle atmosphere," *Rev. Geophys.*, vol. 41, no. 1, pp. 1–64, 2003.

[15] T. Tsuda, S. Kato, and T. Sato, "Observations of inertia-gravity waves in the lower stratosphere using the MU radar," *J. Atmos. Sci.*, vol. 47, no. 3, pp. 370–386, Feb. 1990.

[16] S. K. Satheesh et al., "Vertical distribution of aerosols over Indian region," *J. Geophys. Res. Atmos.*, vol. 104, no. D22, pp. 26821–26833, Nov. 1999.

[17] Y. Bhavani Kumar et al., "Lidar observations of atmospheric boundary layer dynamics over a tropical station," *Curr. Sci.*, vol. 90, no. 8, pp. 1051–1057, Apr. 2006.